

Optical Engineering

OpticalEngineering.SPIEDigitalLibrary.org

Method for the design of nonaxially symmetric optical systems using free-form surfaces

Dmitry Reshidko
Jose Sasian

Method for the design of nonaxially symmetric optical systems using free-form surfaces

Dmitry Reshidko* and Jose Sasian

University of Arizona, College of Optical Sciences, Tucson, Arizona, United States

Abstract. A systematic method for the design of nonaxially symmetric optical systems is described. Free-form optical surfaces are constructed by superposition of a conic segment and a polynomial, and successfully applied to design relatively fast wide field-of-view optical systems. © 2018 Society of Photo-Optical Instrumentation Engineers (SPIE) [DOI: 10.1117/1.OE.57.10.101704]

Keywords: nonaxially symmetric optical systems; free-form surfaces; optical design; aberration correction.

Paper 180171SSP received Jan. 31, 2018; accepted for publication Apr. 24, 2018; published online May 12, 2018.

1 Introduction

Optical systems that do not have axial symmetry can provide useful and unique solutions to certain imaging problems. However, the complexity of the optical design task grows as the degrees of symmetry are reduced and lost: there are more aberration terms to control, and achieving a sharp image over a wide field-of-view (FOV) at fast optical speeds becomes challenging. Plane-symmetric optical systems represent a large family of practical nonaxially symmetric systems that are simple enough to be easily described and thus are well understood. Design methodologies and aberration theory of plane-symmetric optical systems have been discussed in the literature, and various interesting solutions have been reported.¹⁻⁴

The little discussed in the literature technique of confocal systems is effective for the design of nonaxially symmetric optics. A confocal nonaxially symmetric system is constructed in such a way that there is sharp image along a given ray [called the optical axis ray (OAR)] surface after surface. It is possible to show that such a system can have a reduced number of field aberrations, and that the system will behave closer to an axially symmetric system.^{5,6}

In this paper, we review a methodology for the design of nonaxially symmetric optical systems. We utilize an aspherical/free-form surface constructed by superposition of a conic expressed in a coordinate system that is centered on the off-axis surface segment rather than centered on the axis of symmetry, and an XY polynomial. The conic part of the aspherical/free-form surface describes the base shape that is required to achieve stigmatic imaging surface after surface along the OAR. The XY polynomial adds a more refined shape description to the surface sag and provides effective degrees of freedom for high-order aberration correction. This aspheric/free-form surface profile is able to best model the ideal reflective surface and to allow one to intelligently approach the optical design. Examples of two- and three-mirror unobscured wide FOV reflective systems are provided to show how the methods and corresponding aspheric/free-form

surface are applied. We also demonstrate how the method can be extended to design a monolithic free-form objective.⁷

2 Aberrations of Plane-Symmetric Optical Systems

In this section, we review the aberration properties of a plane-symmetric optical system. The well-known concept of the axially symmetric wavefront aberration function $W(\vec{H}, \vec{\rho})$ is extended to describe the imaginary of plane-symmetric systems. The wavefront aberration function $W(\vec{H}, \vec{\rho}, \vec{i})$ of a plane-symmetric optical system gives the geometrical wavefront deformation at the exit pupil as a function of the normalized field \vec{H} , aperture $\vec{\rho}$, and symmetry unit \vec{i} vectors. The plane of symmetry contains a ray, called the OAR that defines the center of the FOV and the center of the pupils. The unit symmetry vector \vec{i} defines the direction of the plane of symmetry. For optical systems that are composed from spherical or slightly aspherical surfaces, the wavefront aberration function is expanded into polynomial series of dot products of the field, aperture, and symmetry unit vectors, and can be written as

$$W(\vec{H}, \vec{\rho}, \vec{i}) = \sum_{k,m,n,p,q} W_{\substack{2k+n+p \\ 2m+n+q \\ n,p,q}} (\vec{H} \cdot \vec{H})^k (\vec{\rho} \cdot \vec{\rho})^m (\vec{H} \cdot \vec{\rho})^n \times (\vec{H} \cdot \vec{i})^p (\vec{\rho} \cdot \vec{i})^q, \quad (1)$$

where each aberration coefficient $W_{2k+n+p, 2m+n+q, n, p, q}$ represents the amplitude of basic wavefront deformation forms defined by the integers k , m , n , p , and q . The sum of these integers represents a certain order of approximation.

The aberration terms to the fourth order of approximation are summarized in Table 1. These terms consist of the well-understood axially-symmetric primary aberrations and an additional set of aberrations that have double-plane and plane symmetry. The magnitude of the aberration coefficients can be calculated from a first-order ray trace and the system structure parameters.¹

The aberration formulas provide insight into the aberration dependence as a function of the system parameters.

*Address all correspondence to: Dmitry Reshidko, E-mail: dreshidko@email.arizona.edu

Table 1 Aberrations of a plane-symmetric optical system. The aberration terms are arranged in groups according to symmetry characteristics.

First group	
W_{00000}	Piston
Second group	
$W_{01001}(\vec{i} \cdot \vec{\rho})$	Field displacement
$W_{10010}(\vec{i} \cdot \vec{H})$	Linear piston
$W_{02000}(\vec{\rho} \cdot \vec{\rho})$	Defocus
$W_{11100}(\vec{H} \cdot \vec{\rho})$	Magnification
$W_{20000}(\vec{H} \cdot \vec{H})$	Quadratic piston
Third group	
$W_{02002}(\vec{i} \cdot \vec{\rho})^2$	Uniform astigmatism
$W_{11011}(\vec{i} \cdot \vec{H})(\vec{i} \cdot \vec{\rho})$	Anamorphic distortion
$W_{20020}(\vec{i} \cdot \vec{H})^2$	Quadratic piston
$W_{03001}(\vec{i} \cdot \vec{\rho})(\vec{\rho} \cdot \vec{\rho})$	Uniform coma
$W_{12101}(\vec{i} \cdot \vec{\rho})(\vec{H} \cdot \vec{\rho})$	Linear astigmatism
$W_{12010}(\vec{i} \cdot \vec{H})(\vec{\rho} \cdot \vec{\rho})$	Field tilt
$W_{21001}(\vec{i} \cdot \vec{\rho})(\vec{H} \cdot \vec{H})$	Quadratic distortion I
$W_{21110}(\vec{i} \cdot \vec{H})(\vec{H} \cdot \vec{\rho})$	Quadratic distortion II
$W_{30010}(\vec{i} \cdot \vec{H})(\vec{H} \cdot \vec{H})$	Cubic piston
$W_{04000}(\vec{\rho} \cdot \vec{\rho})^2$	Spherical aberration
$W_{13100}(\vec{H} \cdot \vec{\rho})(\vec{\rho} \cdot \vec{\rho})$	Linear coma
$W_{22200}(\vec{H} \cdot \vec{\rho})^2$	Quadratic astigmatism
$W_{22000}(\vec{H} \cdot \vec{H})(\vec{\rho} \cdot \vec{\rho})$	Field curvature
$W_{31100}(\vec{H} \cdot \vec{H})(\vec{H} \cdot \vec{\rho})$	Cubic distortion
$W_{40000}(\vec{H} \cdot \vec{H})^2$	Quadratic piston

Moreover, the aberration division into subgroups according to symmetry characteristics reveals the design strategy and indicates the effective degrees of freedom during the optimization process.

An important case to highlight is a plane-symmetric optical system constructed with confocal surfaces such as imaging along the OAR is stigmatic surface after surface. This type of systems has a reduced number of aberrations and potentially can provide better imaging. To satisfy the requirement in the case of reflective systems, surfaces must be off-axis segments of conics. Due to the system construction, there will be no field-independent aberration terms: the surface contributions to spherical aberration (W_{04000}), uniform coma (W_{03001}), and uniform astigmatism (W_{02002}) are all exactly zero. In addition, anamorphic distortion (W_{11011}) and quadratic distortion II (W_{21110}) also nullify, and the surface

contribution to intrinsic anamorphism becomes unity. Moreover, linear astigmatism (W_{12101}) and field tilt (W_{12010}) of the system vanish simultaneously and can be corrected by adjusting the tilt of mirrors. It follows that except for the remaining quadratic distortion I and to the fourth order of approximation, the system behaves as an axially symmetric system.

3 Surface Description

In this section, we present an aspherical/free-form surface in close form that can be used to design plane-symmetric optical systems. We have shown that concatenation of stigmatic components is useful to obtain a starting point for designing a system. A standard tilted and/or decentered axially symmetric conic surface of Eq. (2) provides solution to the problem

$$z(r) = \frac{cr^2}{1 + \sqrt{1 - (1+k)c^2r^2}}, \quad (2)$$

where c is the curvature of the surface, k is the conic constant, and $r = \sqrt{x^2 + y^2}$. However, when one wishes to design a plane-symmetric optical system, it is desirable to have a convenient expression for the surface in a coordinate system that is centered on the off-axis surface segment rather than centered on the axis of symmetry. Some advantages of using this surface description are that the actual surface can be precisely specified, that the system geometry can be easily established and optimized in lens design software, and that additional aspheric terms can be added to provide effective degrees of freedom to further improve the system.

The derivation of the analytical expression of the conic as viewed from a coordinate system that is tangent to the surface at a general point away from the axis of symmetry is reviewed below.^{8,9} Original coordinates (y, z) and new coordinates (y', z') are shown in Fig. 1. Without loss of generality, the new coordinate origin is chosen on the y axis; thus, Y_0 is the distance from the rotation axis to the new coordinate center.

A general expression of an axially symmetric conic surface of Eq. (2) is rewritten as

$$z(r) = \frac{1}{(1+k)} \{R - [R^2 - (1+k) \cdot r^2]^{1/2}\}, \quad (3)$$

where $R = 1/c$ is the radius of curvature of the surface. From Eq. (3), it follows that

$$\tan(\varphi_0) = \frac{\partial z}{\partial y_{x=0; y=Y_0}} = \frac{Y_0}{[R^2 - (1+k) \cdot Y_0^2]^{1/2}}, \quad (4)$$

$$Z_0 = z(0, Y_0) = \frac{1}{(1+k)} \{R - [R^2 - (1+k) \cdot Y_0^2]^{1/2}\}, \quad (5)$$

where φ_0 is the angle of the coordinate system rotation.

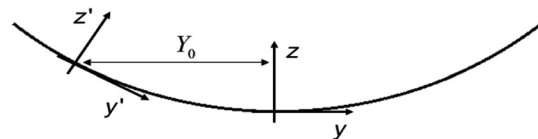


Fig. 1 The geometry defining global and local coordinates of the off-axis conic segment.

The rotation of coordinates is now performed according to

$$x = x', \quad (6)$$

$$y = y' \cos(\varphi_0) - z' \cdot \sin(\varphi_0) + Y_0, \quad (7)$$

$$z = y' \cdot \sin(\varphi_0) + z' \cdot \cos(\varphi_0) + Z_0, \quad (8)$$

$$x' = x, \quad (9)$$

$$y' = (y - Y_0) \cdot \cos(\varphi_0) + (z' - Z_0) \cdot \sin(\varphi_0), \quad (10)$$

$$z' = -(y - Y_0) \cdot \sin(\varphi_0) + (z' - Z_0) \cdot \cos(\varphi_0). \quad (11)$$

For compactness, the dimensionless variables

$$u = \frac{x'}{R}; \quad v = \frac{y'}{R}; \quad w = \frac{z'}{R}; \quad \varepsilon = \frac{Y_0}{R}, \quad (12)$$

and the quantities

$$s \equiv \sin(\varphi_0) = \frac{Y_0}{[R^2 - kY_0^2]^{1/2}},$$

$$c \equiv \cos(\varphi_0) = \left[\frac{R^2 - (k+1)Y_0^2}{R^2 - kY_0^2} \right]^{1/2},$$

$$L \equiv k + 1,$$

$$W_0 \equiv Z_0/R \quad (13)$$

are introduced. Equations (3), (6), (7), (12), and (13) are now substituted into Eq. (8)

$$\frac{1}{L} (1 - L([vc - ws + \varepsilon]^2 + u^2)^{1/2}) = vs + wc + W_0. \quad (14)$$

After some algebraic manipulations, Eq. (14) is reduced to a quadratic equation as in

$$w^2 + 2w(h + jv) - (fv^2 + gu^2) = 0. \quad (15)$$

The solution for $w(u, v)$ is

$$w(u, v) = -(h + jv) \pm [(h + jv)^2 + fv^2 + gu^2]^{1/2}, \quad (16)$$

where $f \equiv (s/\varepsilon)^2 g$, $g \equiv -1/(Lc^2 + s^2)$, $h \equiv (\varepsilon/s)g$ and $j \equiv -(L-1)scg$.

This off-axis conic surface is now used as a base surface to construct an aspherical/free-form surface. The aspherical/free-form surface $z_f(r)$ is constructed by adding a plane-symmetric XY polynomial to the base surface as

$$z_f(r) = w(r) + A_1x^2 + A_2y^2 + A_3x^2y + A_4y^3 + A_5x^4 + A_6x^2y^2 + A_7y^4 \dots, \quad (17)$$

where $w(r)$ is the sag of the base off-axis conic surface, and A_i 's are the aspheric polynomial coefficients. The XY polynomial in Eq. (17) is centered at the origin of the off-axis conic segment and thus provides effective degrees of freedom for the correction of off-axis aberrations. This very

ad hoc surface allows for optimum design or to refine the design performance of plane-symmetric refractive systems.

4 Design Method

In this section, we outline a systematic method to the design of plane-symmetric reflective systems that utilizes the aspheric/free-form surface defined in Sec. 3.

1. A well-corrected axially symmetric system provides an initial estimate for the first-order parameters and serves as a good starting point for a nonaxially symmetric design. All surfaces are axially symmetric conics and imaging is stigmatic along the optical axis surface after surface.
2. Axially symmetric conic surfaces are converted into aspheric/free-form surfaces. A plane-symmetric form is generated by tilting the system elements in a plane and adding the off-axis conic decenter parameter Y_0 (see Fig. 1) into optimization. Optimization variables are the surface tilts and separations, and parameter Y_0 . Structure constraints are assigned, and the system is reoptimized to obtain stigmatic imaging along the OAR.
3. Several points in the FOV of the system are added, and the tilt of the last mirror is adjusted to correct linear astigmatism.
4. At this point, the base conic surface is frozen, and only aspheric polynomial coefficients are used by the optimizer as degrees of freedom to correct off-axis aberrations. The coefficients are released as variables and as the optimizer proceeds, more coefficients are released.

Usually, there are several ways to set up a decentered or tilted element in lens design software. We choose a way that is simple to understand, allows to easily construct a system with confocal surfaces, and permits a minimum number of tilt or decenter parameters.

In software, when we tilt and/or decenter a surface, we are actually tilting and/or decentering the local coordinate system in which the surface is defined. Each aspheric/free-form surface is sandwiched between two coordinate breaks with the same tilt angle. The surface is tilted, and the coordinate system is tilted again to follow the beam before translating to the next surface. As a result, the OAR is aligned with the surface vertex of each aspherical/free-form surface which allows to effectively control high-order aberrations and to achieve balance performance over the entire field by introducing small asphericities as effective degrees of freedom in step 4. In addition by sandwiching the free-form surface between two coordinate breaks, the OAR becomes aligned with the z -axis of the second coordinate system and the OAR passes through the center of the image plane. This scheme also helps to cleanly define the geometry of a plane symmetric system.

The surface $z_f(r)$ in Eq. (17) was programmed as a user-defined surface in Zemax OpticStudio optical design software and was successfully applied to design several plane-symmetric optical systems. In the following sections, we will present design examples of two- and three-mirror unobscured telescopes. Finally, we will extend our design method to refractive optical systems and show an example of a monolithic free-form objective.

5 Two-Mirror Unobscured Telescope

In this section, we show a step-by-step design process of a two-mirror unobscured Schwarzschild-type telescope using the systematic method outlined in Sec. 3. We start with an axially symmetric system shown in Fig. 2(a). In this design, curvatures and conic constants of the mirrors are chosen such that imaging on axis is stigmatic surface after surface. The primary mirror is parabolic, and the secondary mirror is hyperbolic. The system operates at $f/4$. The optical path difference (OPD) plots for 0 and ± 2 deg fields are shown in Fig. 2(b). The off-axis performance is considerably degraded by coma, field curvature, and astigmatism.

A plane-symmetric form can be generated by simply tilting and decentering the system elements in a plane. However, if surfaces are defined as standard axially symmetric conic surfaces, only a small off-axis segment of the actual surface is used to bend rays as shown in Fig. 3(a). Notice that in this case aspherical polynomial defined with respect to the surface vertex does not provide effective degrees of freedom for further optimization as high-order polynomial terms are required to produce small aspheric departures at

the surface off-axis segment. On the other hand, optical systems, which contain lens elements that use higher order aspheric terms, are subjected to produce oscillation on the ray behavior and are susceptible to creating imaging artifacts when they are slightly misaligned.

Instead, axially symmetric conic surfaces are converted into aspheric/free-form surfaces $z_f(r)$. This surface description simplifies the design by allowing one to set the offset parameter Y_0 for a given mirror so that stigmatic imaging along the OAR is obtained. The optimization variables are the surface tilts (angle of incidence of the OAR) and surface separations along the OAR, and the parameter Y_0 . The image plane is constrained to be perpendicular to the OAR, and as the system changes it is reoptimized to correct aberrations on axis. The layout is shown in Fig. 3(b). The OPD plots of this plane-symmetric system are shown in Fig. 4. Notice that due to the system construction, there is no field-independent aberration terms. Once the tilt of the secondary mirror is adjusted to correct linear astigmatism and field tilt, the system performs close to the corresponding axially symmetric system.

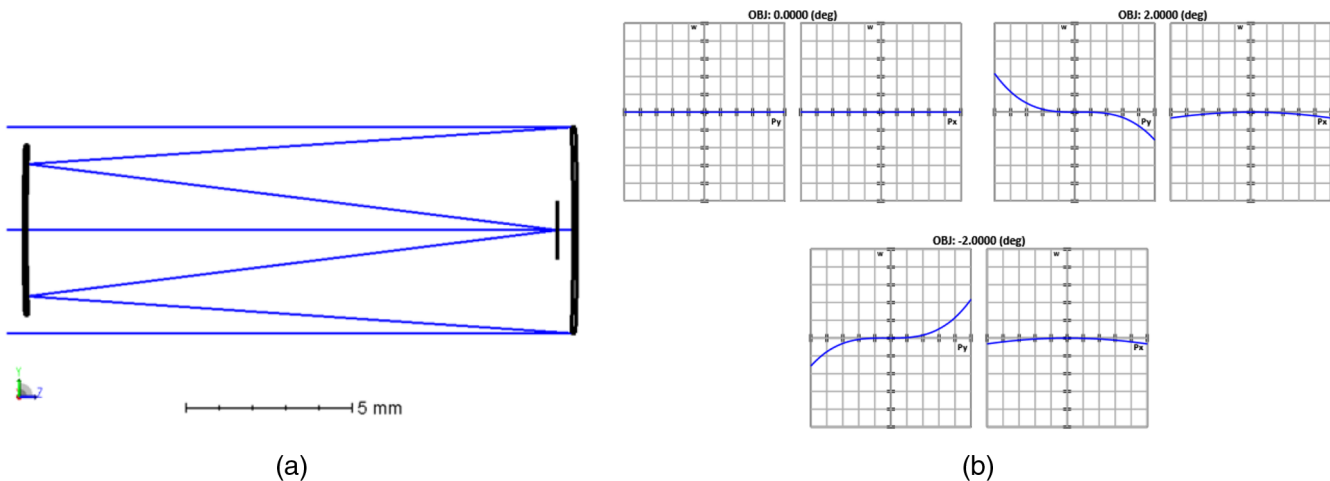


Fig. 2 The starting design of a two-mirror unobscured Schwarzschild-type telescope. (a) Layout and (b) OPD plots (plot scale is 2 waves at $0.550 \mu\text{m}$). In this design, imaging on-axis is stigmatic surface after surface.

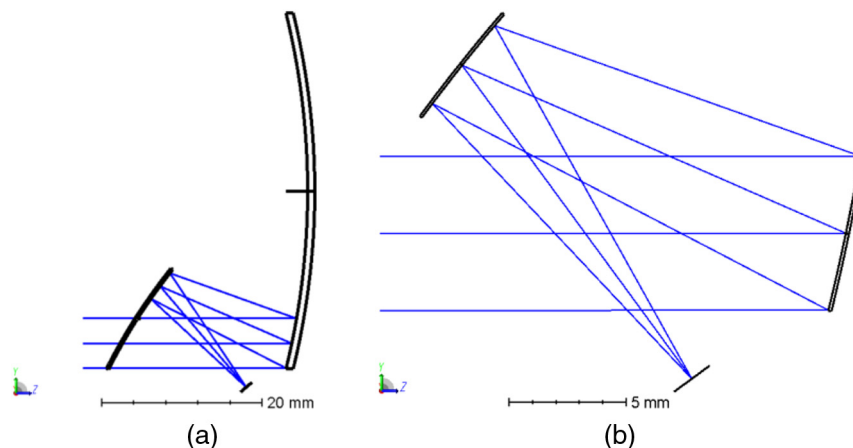


Fig. 3 The elements are tilted and/or decentered to generate an unobscured optical system. Mirror surfaces are defined with (a) standard axially symmetric conic surfaces and (b) aspheric/free-form surfaces $z_f(r)$.

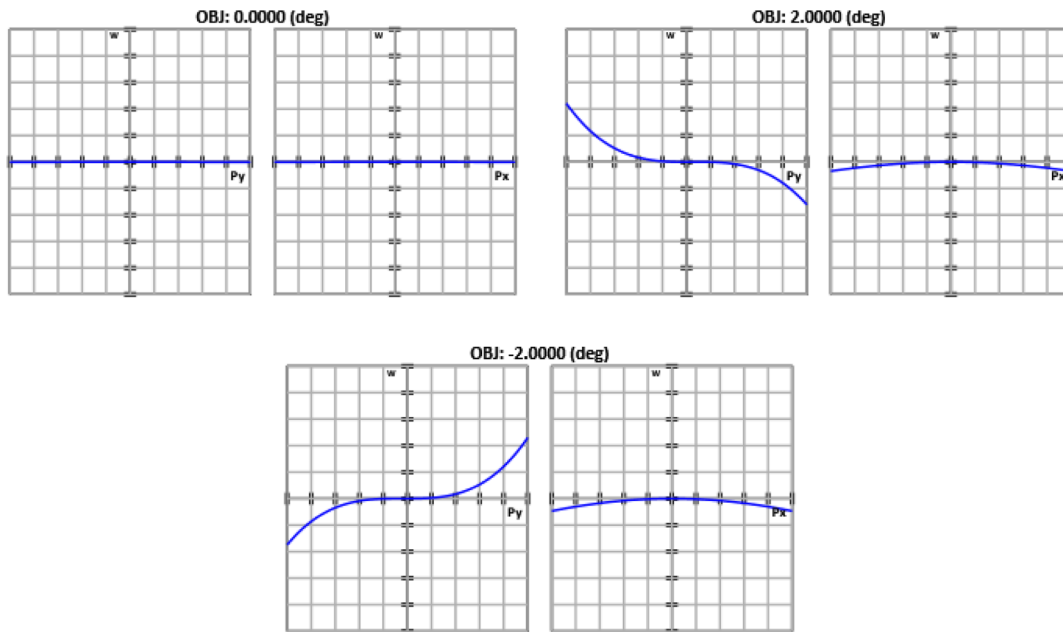


Fig. 4 OPD plots of the unobscured telescope (plot scale is two waves at $0.550 \mu\text{m}$). The plane-symmetric system designed with confocal surfaces performs close to the corresponding axially symmetric system.

Off-axis aberrations are now corrected by adding aspheric polynomial coefficients to the optimization. System geometry, surface curvatures, and conic constants are locked, and aspheric coefficients are released as variables. The FOV is gradually increased, and more coefficients are released as the optimizer proceeds. The final system, presented in Fig. 5, covers an FOV of 6×4 degrees at $f/4$. The OPD plots and full-field spot diagram are shown in Fig. 6. Uniform image quality and close to diffraction limited performance have been achieved over the entire FOV. For reference, two-mirror

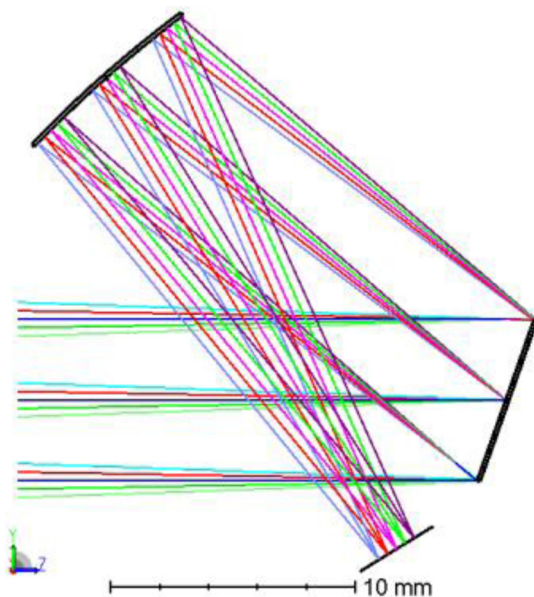


Fig. 5 Layout of the final two-mirror unobscured Schwarzschild-type telescope design. Aspheric polynomial terms are used to correct off-axis aberrations.

unobscured telescopes designed with standard conic and aspheric surfaces provide diffraction limited performance over an FOV of only few degrees.³

6 Three-Mirror Unobscured Telescope

In this section, we present an $f/2$ three-mirror unobscured telescope design that closely resembles the nonuniform rational-basis spline (NURBS) free-form design reported by Chrisp and show the performance improvement made by using aspheric surfaces $z_f(r)$.¹⁰ The design parameters are given in Table 2.

The design procedure is similar to one used in the previous section. The initial system is constructed with confocal surfaces, as shown in Fig. 7(a). Mirror sizes, separations, and incidence angles were chosen to closely match the NURBS design by Chrisp. Notice that linear astigmatism and field tilt are removed by adjusting the tilt of the tertiary mirror, as shown in Fig. 7(b).

Next, mirror curvatures, conic constants, and surface separations are removed from the optimization, and up to eighth-order plane-symmetric polynomial coefficients are added as variables to correct off-axis aberrations. Although no constraints on distortion were mentioned by Chrisp, in the current design the distortion is limited to $<3\%$. The system layout reproduced from the paper by Chrisp and our final system layout are presented side by side in Fig. 8. The OPD plots and spot diagrams of our system are given in Fig. 9. The performance is close to being diffraction-limited over the entire FOV.

In his paper, Chrisp compared the performance of the design with NURBS surfaces to designs that use conventional tilted and/or decentered rotational aspheres, and XY polynomials. The RMS spot size over the field for different designs is shown in Fig. 10. Chrisp reported the average RMS spot size over the field to be $61 \mu\text{m}$ for the conventional

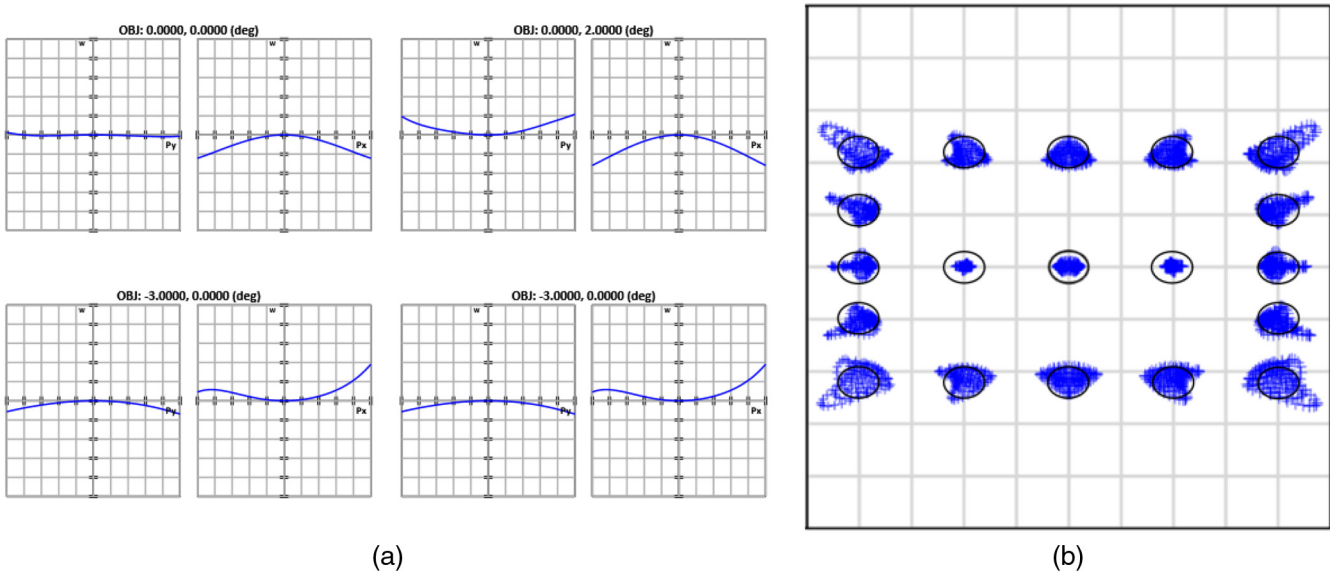


Fig. 6 Imaging performance of the final two-mirror unobscured Schwarzschild-type telescope design. (a) OPD plots (plot scale is 1 wave at $0.550 \mu\text{m}$) and (b) full-field spot diagram at $0.550 \mu\text{m}$. Close to diffraction limited performance over an FOV of 6×4 deg was achieved.

Table 2 Design requirements for the three-mirror unobscured system.

Parameter	Requirement
FOV	10×9 deg
Focal length	35.7 mm
Focal ratio	$f/2$

aspheric design, $36 \mu\text{m}$ for the XY polynomial design, and $14 \mu\text{m}$ for the NURBS design. In the current design, the average RMS spot is $8.5 \mu\text{m}$, which is about 40% better comparing to the NURBS design.

Although the design presented by Chrisp shows excellent performance, the surface representation with NURBS has a number of disadvantages. The major optical design programs are not capable of optimizing NURBS grid-type surfaces in imaging systems. For this reason, the optimization of the design by Chrisp was accomplished with an in-house code. Moreover, the NURBS design represents a “brute force”/“number crunching” solution, whereas the aspheric surface

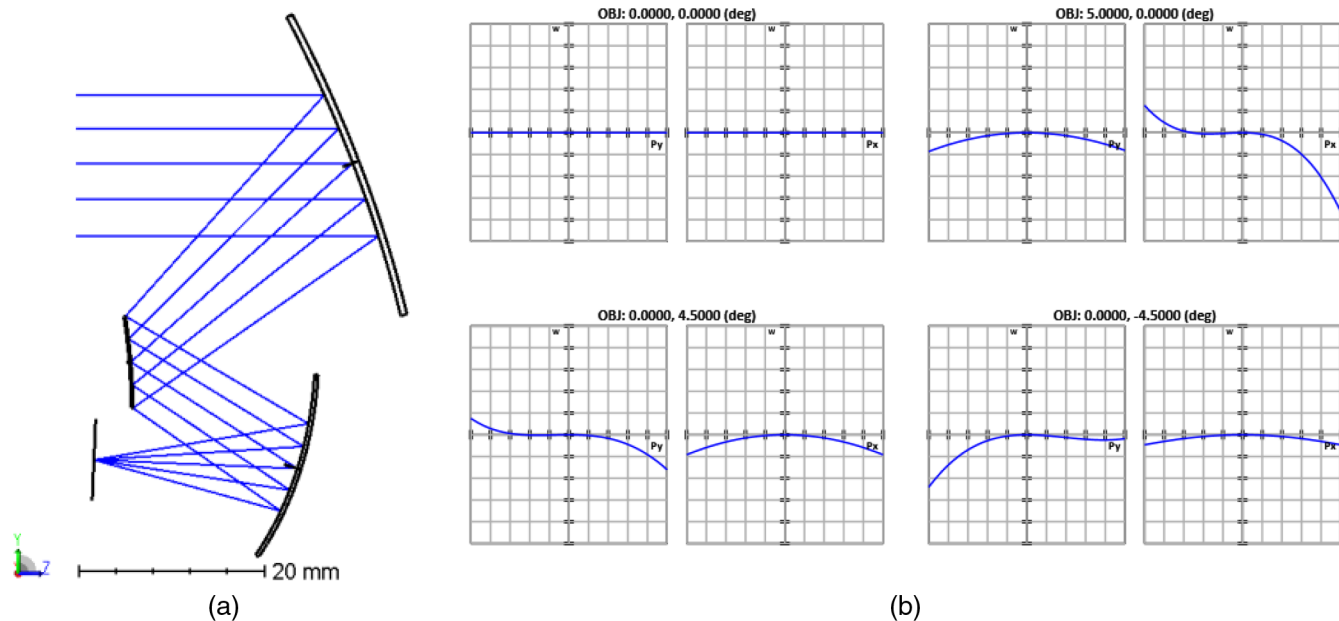


Fig. 7 The starting design of a three-mirror telescope is constructed with confocal surfaces. (a) Layout and (b) OPD plots (the plot scale is 10 waves at $3 \mu\text{m}$). In this design, imaging on-axis is stigmatic surface after surface. Tilt of the tertiary mirror is adjusted to correct field tilt and linear astigmatism.

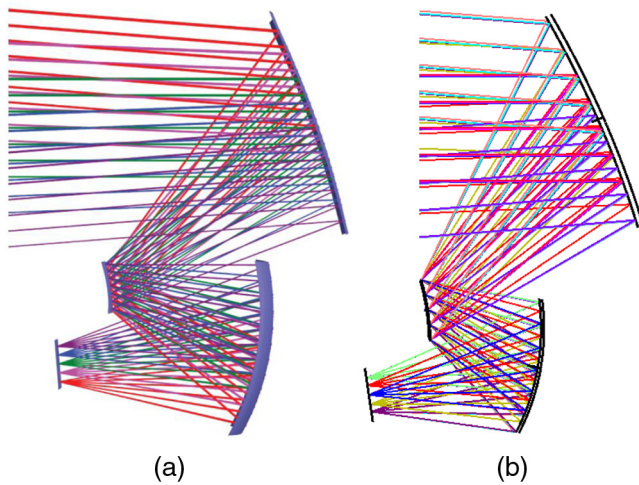


Fig. 8 Layout of the three-mirror telescope. (a) The design with NURBS free-form surfaces reported by Chrisp; (b) the current design with aspherical/free-form surfaces $z_f(r)$. In the current design, up to eighth-order plane-symmetric polynomials are used to correct off-axis aberrations.

profile of the mirrors $z_f(r)$ is clearly able to best model the required ideal surface and to allow one to intelligently approach the optical design.

7 Monolithic Free-form Objective

So far, we have discussed the design of reflective plane-symmetric optical systems. In this section, we extend our design method to refractive optical systems and show an additional free-form surface constructed by superposition of a Cartesian oval surface and polynomial.

The Cartesian oval is an optical surface that separates two homogeneous refracting media and produces a perfect point image of a point object. In the special case of a mirror surface in which the index of refraction of object and image space media have the same magnitude but the opposite sign,

the Cartesian oval solutions are conic surfaces. Other well-known solutions are a sphere for the case of aplanatic and concentric conjugate points or conic surface with the conic constant equal to the minus square of the index of refraction for the case of having one conjugate point at infinity. However, a general sag equation of the Cartesian oval is complicated. The solution for the explicit sag of the Cartesian oval has been previously discussed by other authors. Moreover, an alternate iterative method for the sag of the Cartesian oval has also been provided.¹¹

This iterative method solves the defining optical path length equation for the Cartesian oval for any ray from the object point O to the image point O' , as shown in Fig. 11

$$\text{OPL}_p - \text{OPL}_{\text{axis}} = \left\{ n_1 \cdot \sqrt{[s_1 + S_c(r)]^2 + r^2} + n_2 \cdot \sqrt{[s_2 - S_c(r)]^2 + r^2} \right\} - \{n_1 \cdot s_1 + n_2 \cdot s_2\} = 0, \quad (18)$$

where $S_c(r)$ is the sag of the Cartesian oval, n_1 and n_2 are the indices of refraction in object and image spaces, and s_1 and s_2 are the object and image distances from the surface vertex, respectively.

The Cartesian oval has the property of perfectly imaging an object point into an image point with any numerical aperture. However, the imaging performance of the Cartesian oval degrades rapidly for off-axis field positions. Similarly to the construction of the aspheric/free-form surface $z_f(r)$, the aspherical surface $z_c(r)$ is now constructed by adding a polynomial to the base surface $S_c(r)$ as

$$z_c(r) = S_c(r) + A_1 r^4 + A_2 r^6 + A_3 r^8 + \dots, \quad (19)$$

where the A 's represent the aspheric polynomial coefficients. A combination of surfaces $z_f(r)$ and $z_c(r)$ can be used to design certain plane-symmetric systems.

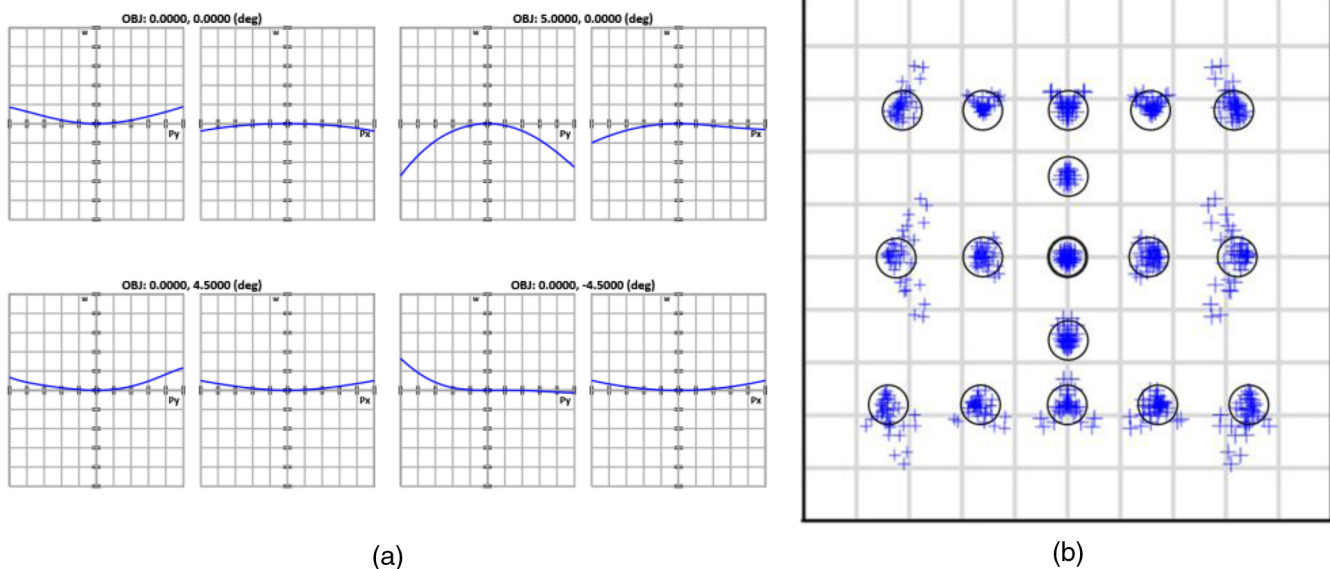


Fig. 9 Imaging performance of the final three-mirror telescope. (a) OPD plots (the plot scale is 1 wave at $3 \mu\text{m}$) and (b) spot diagrams at $3 \mu\text{m}$. Close to diffraction limited performance over an FOV of 10×9 deg was achieved.

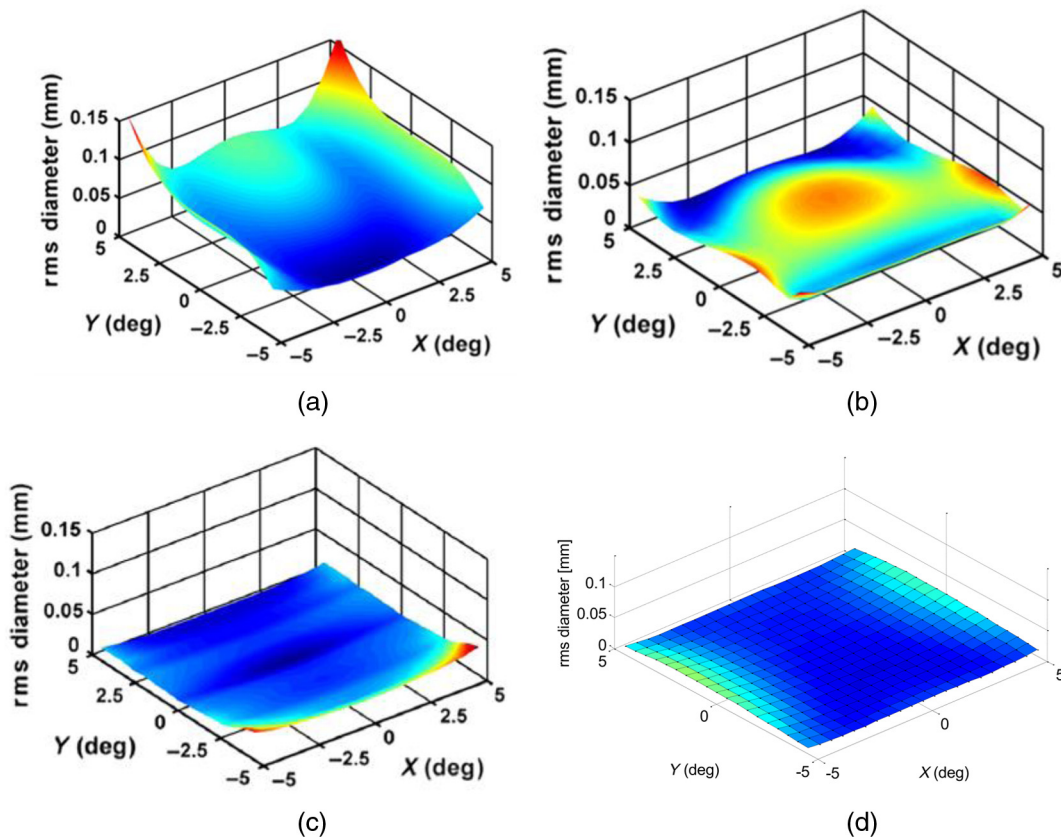


Fig. 10 The RMS Spot Size over the field of the three-mirror system. (a) The design with conventional aspheric surfaces reported by Chrisp, (b) the design with XY polynomial surfaces reported by Chrisp, (c) the design with NURBS free-form surfaces reported by Chrisp, and (d) the current design with aspherical surfaces $z_f(r)$.

As an example, we present a monolithic free-form objective that closely resembles the monolithic free-form objective design discussed by Kiontke.¹² The design covers a vertical FOV of about 25 deg at $f/1.4$ and operates in the long-wave infrared region. The monolithic objective is made of germanium. The initial system is constructed with confocal surfaces and comprises a free-form surface $z_c(r)$ to couple light from the object into the material, two free-form/aspherical surfaces $z_f(r)$ to bend light in the material, and additional free-form surface $z_c(r)$ to out-couple light toward the detector, as shown in Fig. 12.

Next, the Cartesian oval parameters (s_1 and s_2), mirror curvatures, conic constants, and separations are removed

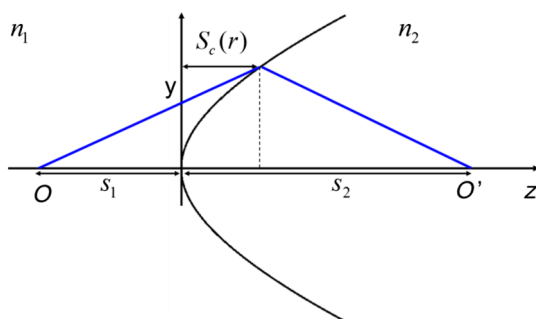


Fig. 11 Geometrical variables used to define the Cartesian oval surface. All rays from the object point O to the image point O' have equal optical path length.

from the optimization, and polynomial coefficients are released as variables to balance off-axis aberrations. The system layout reproduced from the paper by Kiontke and our final system layout are presented side by side in Fig. 13. The OPD plots and spot diagrams of our system are given in Fig. 14. Excellent, balanced performance over an FOV of 37×25 deg has been achieved.

The design reported by Kiontke utilizes three axially symmetric aspheric surfaces and one free-form surface. The free-form surface is described as a superposition of Zernike polynomials and is used to compensate plane-symmetric aberrations. These aspheric and free-form surface descriptions are widely accepted. However, selecting a starting point for the design, satisfying all geometrical constraints, and compensating for aberrations induced by breaking up the rotational symmetry of the optical system impose challenges for the optical design. In the current design, the system geometry has already been established during the initial design step. By construction, the initial system has a reduced number of field aberrations, and only small aspheric departures to the surface sag are required to effectively correct off-axis aberrations.

8 Conclusion

To summarize, we review the methodology for the design of plane-symmetric optical systems and demonstrate an aspheric/free-form surface profile $z_f(r)$ constructed by superposition of a conic segment and polynomial. We also

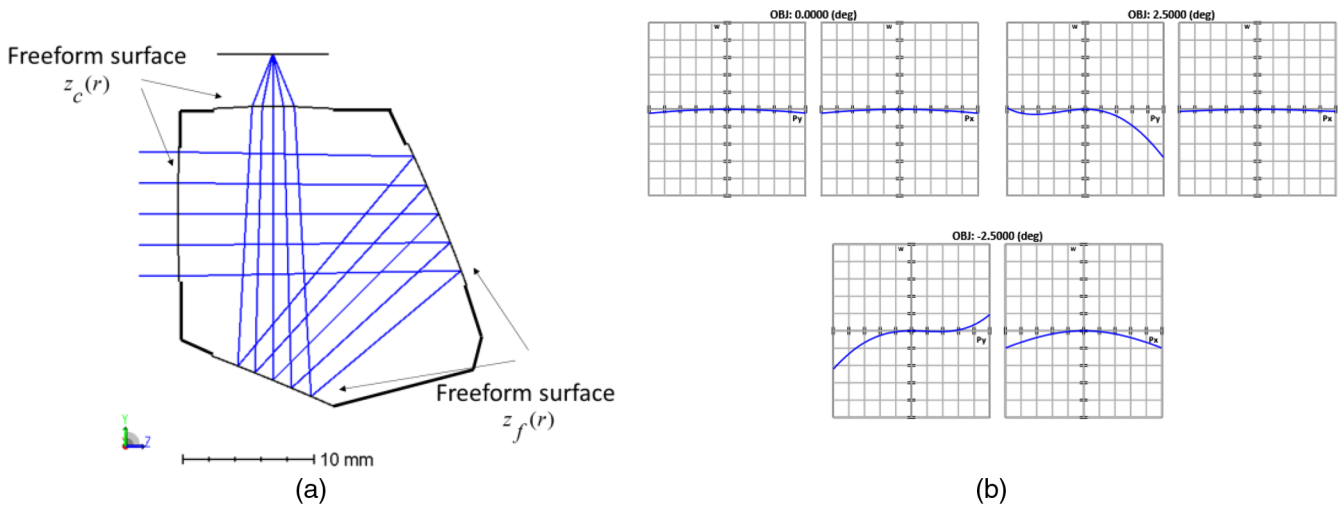


Fig. 12 The starting design of a monolithic free-form objective is constructed with confocal surfaces. (a) Layout and (b) OPD plots (the plot scale is 5 waves at $9 \mu\text{m}$). Combination of free-form surfaces $z_f(r)$ and $z_c(r)$ allows to achieve stigmatic imaging on-axis surface after surface.

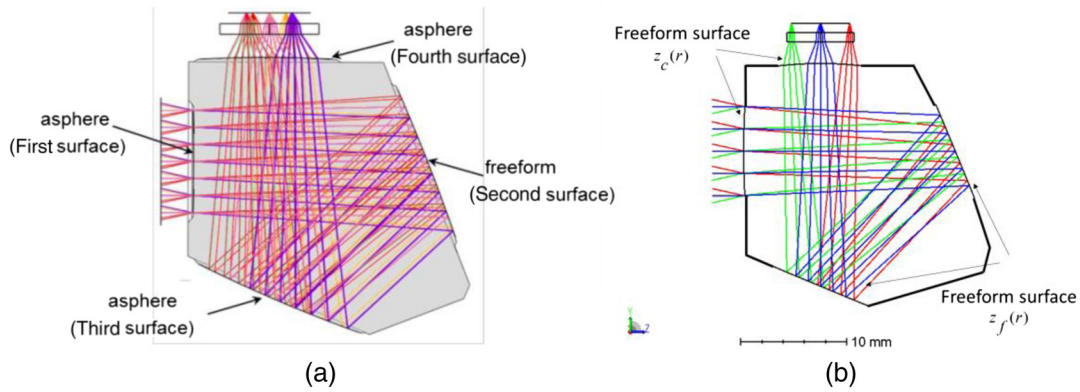


Fig. 13 Layout of the monolithic objective design. (a) The design with aspheric and Zernike free-form surfaces reported by Kiontke and (b) the current design with aspherical/free-form surfaces $z_f(r)$ and $z_c(r)$. In the current design, aspheric polynomials are used to correct off-axis aberrations.

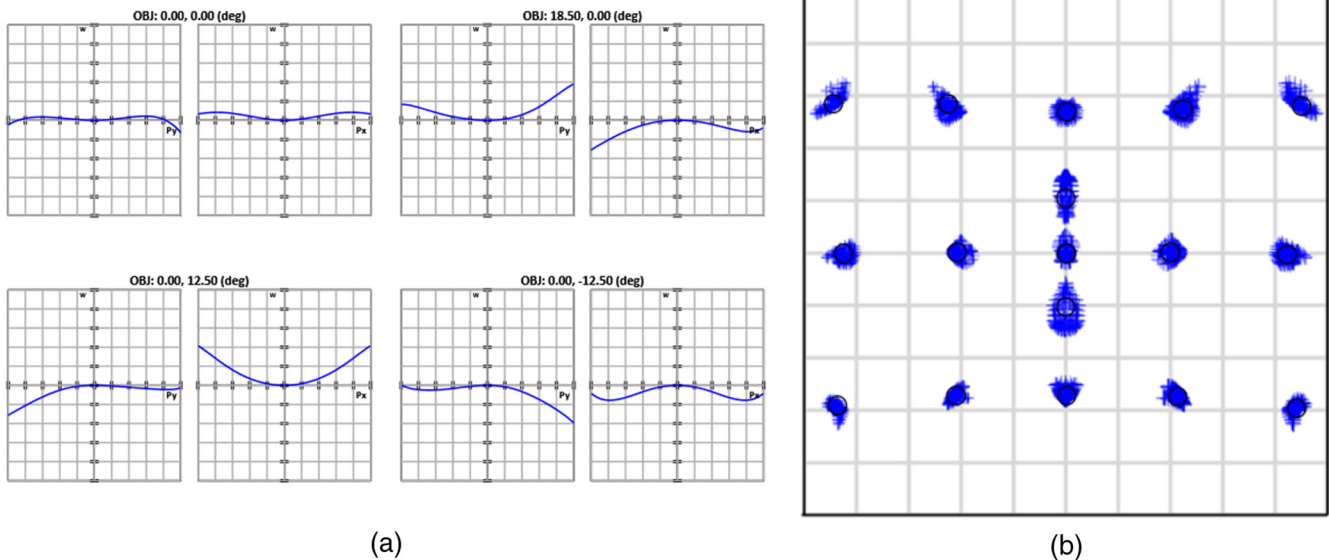


Fig. 14 Imaging performance of the final monolithic objective design. (a) OPD plots (the plot scale is 1 wave at $9 \mu\text{m}$) and (b) spot diagrams at $9 \mu\text{m}$. Excellent, balanced performance over an FOV of 37×25 deg was achieved.

show an aspheric surface profile $z_c(r)$ constructed by superposition of a Cartesian oval and polynomial.

The surfaces $z_f(r)$ and $z_c(r)$ are useful for designing plane-symmetric systems, where the imaging is stigmatic surface after surface along the OAR. Such systems have a reduced number of field aberrations and behave closer to an axially symmetric system. Moreover, these surfaces provide additional degrees of freedom to balance aberration for the off-axis field positions and allow one to compensate for aberrations induced by breaking up the rotational symmetry of the system.

A systematic method is shown that provides a practical and effective means for establishing a starting design point and allows one to design relatively fast wide FOV plane-symmetric systems. We found that this specific method and corresponding aspheric/free-form surface significantly simplify the optical design task. The method has been successfully applied to design two- and three-mirror unobscured wide FOV reflective systems, and a monolithic free-form objective. Excellent performance over a large FOV has been achieved. The method can be extended to systems with surface tilts in two directions.

The surfaces $z_f(r)$ and $z_c(r)$ allow for optimum design or to refine the design performance of plane-symmetric optical systems by enabling a design with equivalent performance but a faster focal ratio or larger FOV than a design with convention surfaces.

The free-form surfaces demonstrated in this paper are not trivial to manufacture and test. However, recent technological improvements have allowed for production of similar free-form components. For example, additional axes of machine tool control and advancements in postprocessing of components have extended diamond-turning manufacturing capabilities.^{10,12}

References

1. J. M. Sasian, "How to approach the design of a bilateral symmetric optical system," *Opt. Eng.* **33**(6), 2045–2061 (1994).
2. J. Sasian, "Optical design of refractive wide-field cameras," *Proc. SPIE* **7060**, 70600C (2008).
3. J. M. Rogers, "Unobscured mirror design," *Proc. SPIE* **4832**, 33–61 (2002).
4. J. Sasian, "Design of a Schwarzschild flat-field, anastigmatic, unobstructed, wide-field telescope," *Opt. Eng.* **29**(1), 1–6 (1990).
5. J. M. Sasian, "Review of methods for the design of unsymmetrical optical systems," *Proc. SPIE* **1396**, 453–466 (1990).
6. J. R. Rogers, "Techniques and tools for obtaining symmetrical performance from tilted-component systems," *Opt. Eng.* **39**(7), 1776–1788 (2000).
7. D. Reshidko and J. Sasian, "A method for the design of unsymmetrical optical systems using freeform surfaces," *Proc. SPIE* **10590**, 105900V (2017).
8. J. Nelson and M. Temple-Raston, "The off-axis expansion of conic surfaces," UC TMT Report No. 91 (1982).
9. D. Reshidko, "Topic in modern lens design," PhD Dissertation, College of Optical Sciences, University of Arizona (2016).
10. M. Chrisp, "New freeform NURBS imaging design code," *Proc. SPIE* **9293**, 92930N (2014).
11. C. Hsueh et al., "Closed-form sag solutions for Cartesian oval surfaces," *J. Opt.* **40**(4), 168–175 (2011).
12. S. R. Kiontke, "Monolithic freeform element," *Proc. SPIE* **9575**, 95750G (2015).

Dmitry Reshidko is a PhD candidate whose research involves development of novel imaging techniques and methods for image aberration correction, innovative optical design, fabrication, and testing of state-of-the-art optical systems.

Jose Sasian is a professor at the University of Arizona. His interests are in teaching optical sciences, optical design, illumination optics, optical fabrication and testing, telescope technology, opto-mechanics, lens design, light in gemstones, optics in art and art in optics, and light propagation. He is a fellow of SPIE and the Optical Society of America, and is a lifetime member of the Optical Society of India.